



## OPEN PSD3, regulated by PKM2, endows growth and metastasis advantages in esophageal squamous cell carcinoma by modulating EMT progression

Qiqi Zhang<sup>1,2,6</sup>, Qing Liu<sup>1,6</sup>, Shutao Zheng<sup>1</sup>, Tao Liu<sup>3</sup>, Lifei Yang<sup>4</sup>, Yiyi Tan<sup>1</sup> & Xiaomei Lu<sup>1,5</sup>✉

PH and Sect. 7 domain-containing protein 3 (PSD3) has been reported to be associated with some cancers, but its role in esophageal squamous cell carcinoma (ESCC) has not been thoroughly examined. The purpose of this study was to investigate the expression of PSD3 in ESCC and determine whether PSD3 is regulated by pyruvate kinase type M2 (PKM2) to affect the malignant phenotype of ESCC cells. First, we found that PSD3 was highly expressed in ESCC tissues and correlated with ESCC lymph node metastasis. In vitro, PSD3 promoted the proliferation, migration and invasion of ESCC cells. In vivo, PSD3 accelerated ESCC growth and metastasis. Next, the interaction between PSD3 and PKM2 was examined, and the results showed that PSD3 was directly regulated by PKM2. Functionally, PSD3 was regulated by PKM2 to promote the proliferation, migration and invasion of ESCC cells. Mechanistically, PSD3 was regulated by PKM2 to upregulate the expression of Vimentin and Snail and downregulate the expression of E-cadherin. Collectively, all the data we show here demonstrate that PSD3, regulated by PKM2, endows growth and metastasis advantages in ESCC by modulating epithelial-mesenchymal transition (EMT) progression.

**Keywords** EMT, ESCC, Metastasis, PSD3, PKM2

Esophageal carcinoma (ESCA) is a malignant tumor of the upper digestive tract and includes esophageal squamous cell carcinoma (ESCC) and esophageal adenocarcinoma (EAC). Esophageal squamous cell carcinoma (ESCC) has historically been prevalent in China, and the overall 5-year survival rate is less than 20%<sup>1</sup>. Although some targeted anticancer drugs, such as gefitinib and PD-L1 blockers<sup>2,3</sup> have been adopted in the clinic, the mortality rate of ESCC is still relatively high owing to invasion, distant metastasis. Therefore, it is critical and necessary to understand the underlying molecular mechanisms of invasion and metastasis.

PH and Sect. 7 domain-containing protein 3 (PSD3), a guanine nucleotide exchange factor (GEF), activates ADP-ribosylation factor 6 (ARF6) and is localized in the plasma membrane<sup>4</sup>. PSD3 contains a Sect. 7 domain, a PH domain, and a C-terminal domain. The Sect. 7 domain is responsible for its ARF-GEF activity, the PH domain is responsible for its plasma membrane localization and interaction with phosphatidylinositol (PI), and the C-terminal domain is responsible for downstream signaling protein interactions and cytoskeletal rearrangement<sup>5</sup>. This suggests that PSD3 may play a critical role in various cellular events, such as actin cytoskeleton remodeling and endocytosis<sup>6</sup>. PSD3 was originally identified as tumor-associated antigen 67 in hepatocellular carcinoma<sup>7</sup> and was reported to be involved in hepatocyte growth factor (HGF)-dependent ARF6

<sup>1</sup>State Key Laboratory of Pathogenesis, Prevention and Treatment of High Incidence Diseases in Central Asia, Clinical Medical Research Institute, The First Affiliated Hospital of Xinjiang Medical University, Xinjiang Uygur Autonomous Region, Urumqi 830000, China. <sup>2</sup>Second Department of Gastroenterology, The First Affiliated Hospital of Xinjiang Medical University, Xinjiang Uygur Autonomous Region, Urumqi 830000, China. <sup>3</sup>Department of Clinical Laboratory, The First Affiliated Hospital of Xinjiang Medical University, Xinjiang Uygur Autonomous Region, Urumqi 830000, China. <sup>4</sup>First Department of Lung Cancer Chemotherapy, Cancer Hospital Affiliated with Xinjiang Medical University, Xinjiang Uygur Autonomous Region, Urumqi 830000, China. <sup>5</sup>Xinjiang Branch of Key Laboratory of Cancer Immunotherapy and Radiotherapy, Chinese Academy of Medical Sciences, Xinjiang Uygur Autonomous Region, Urumqi 830000, China. <sup>6</sup>These authors contributed equally: Qiqi Zhang and Qing Liu. ✉email: luxiaomei88@163.com



Characteristics	Cases	PSD3 expression		$\chi^2$	<i>p</i>
		High	Low		
Type					
ESCC	114	83	31	35.192	0.000
NAT	66	18	48		
Gender					
Male	84	65	19	3.373	0.066
Female	30	18	12		
Age (year)					
≥ 60	83	59	24	0.458	0.499
< 60	31	24	7		
Differentiation degree					
Well	8	8	0	5.631	0.060
Moderate	82	61	21		
Poor	24	14	10		
T classification					
T1-T2	29	19	10	1.044	0.307
T3-T4	85	64	21		
N classification					
N <sub>0</sub>	53	33	20	5.561	0.018
N <sub>1</sub> -N <sub>3</sub>	61	50	11		
Gross classification type					
Ulcerative	70	50	20	4.565	0.169
Protrude	7	3	4		
Medullar	33	26	7		
Shrinkage	4	4	0		

**Table 1.** Clinicopathological significance of PSD3 expression in ESCC by  $\chi^2$  test. ESCC, esophageal squamous cell carcinoma; NAT, normal adjacent tissue; PSD3, pleckstrin and Sect. 7 domain containing 3.

### PSD3 promotes the proliferation, migration, and invasion of ESCC cells in vitro

To understand the biological roles of PSD3 in the growth and motility of ESCC cells, the detection of PSD3 was extended from clinical tissues to in vitro cell lines. As shown in Fig. 2A, among the ESCC cell lines, Eca-109 cells exhibited relatively low PSD3 expression, and PSD3 expression was highest in KYSE-150 cells. Western blot analysis showed that Lv-overexpress-PSD3 transduction resulted in significant overexpression of PSD3 and that Lv-shRNA-PSD3-1 transduction successfully resulted in significant depletion of PSD3 (Fig. 2B, C). Therefore, Lv-shRNA-PSD3-1 was used to knock down PSD3 in subsequent experiments. Next, changes in the proliferation, migratory and invasive abilities of ESCC cells after artificial manipulation of PSD3 expression were evaluated by MTT, Wound Healing and Transwell assays, respectively. Results showed that PSD3 promoted the proliferation (Fig. 2D), migration (Fig. 2E, F) and invasion (Fig. 2F) of ESCC cells.

### PSD3 promotes the growth and metastasis of ESCC tumors in vivo

Considering that there are distinct physiological differences between in vitro and in vivo conditions, we next confirmed the effects of PSD3 on tumor growth and metastasis in vivo. The results showed that PSD3 significantly promoted the growth of tumor lesions (Fig. 3A-C) and increased the level of luciferase in nude mice (Fig. 3D). In conclusion, PSD3 promotes the growth and metastasis of ESCC tumors in vivo.

### PSD3 facilitates the EMT process in ESCC

We next explored the possible mechanism of action of PSD3 in the progression of ESCC. First, analysis of the GEPIA database showed that *CDH1* (E-cadherin) and *Vim* (Vimentin) were associated with *PSD3* in squamous cell carcinoma (SCC) (Supplementary Fig. 0.1 A, B). Second, EMT-related proteins were evaluated by Western blot after PSD3 expression was artificially manipulated. As shown in Fig. 4A, PSD3 affected the expression of E-cadherin, Vimentin and Snail, and this pattern was further confirmed by immunofluorescence experiments (Fig. 4B). This suggests that PSD3 promotes the EMT process in vitro. We next attempted to confirm the observation in vivo (Fig. 4C and Supplementary Fig. 1 C). Together, these data demonstrate that PSD3 promotes tumor growth and metastasis in vitro and in vivo by regulating the EMT process.

### PSD3 is directly regulated by PKM2

Based on the above results, we recognized that PSD3 promotes ESCC growth and metastasis and that PSD3 may be regulated by PKM2, but the specific relationship between PSD3 and PKM2 remains unclear. PKM2 expression was evaluated in the ESCC tissue microarray HEso-Squ180Sur-01 in our previous study<sup>16</sup> while

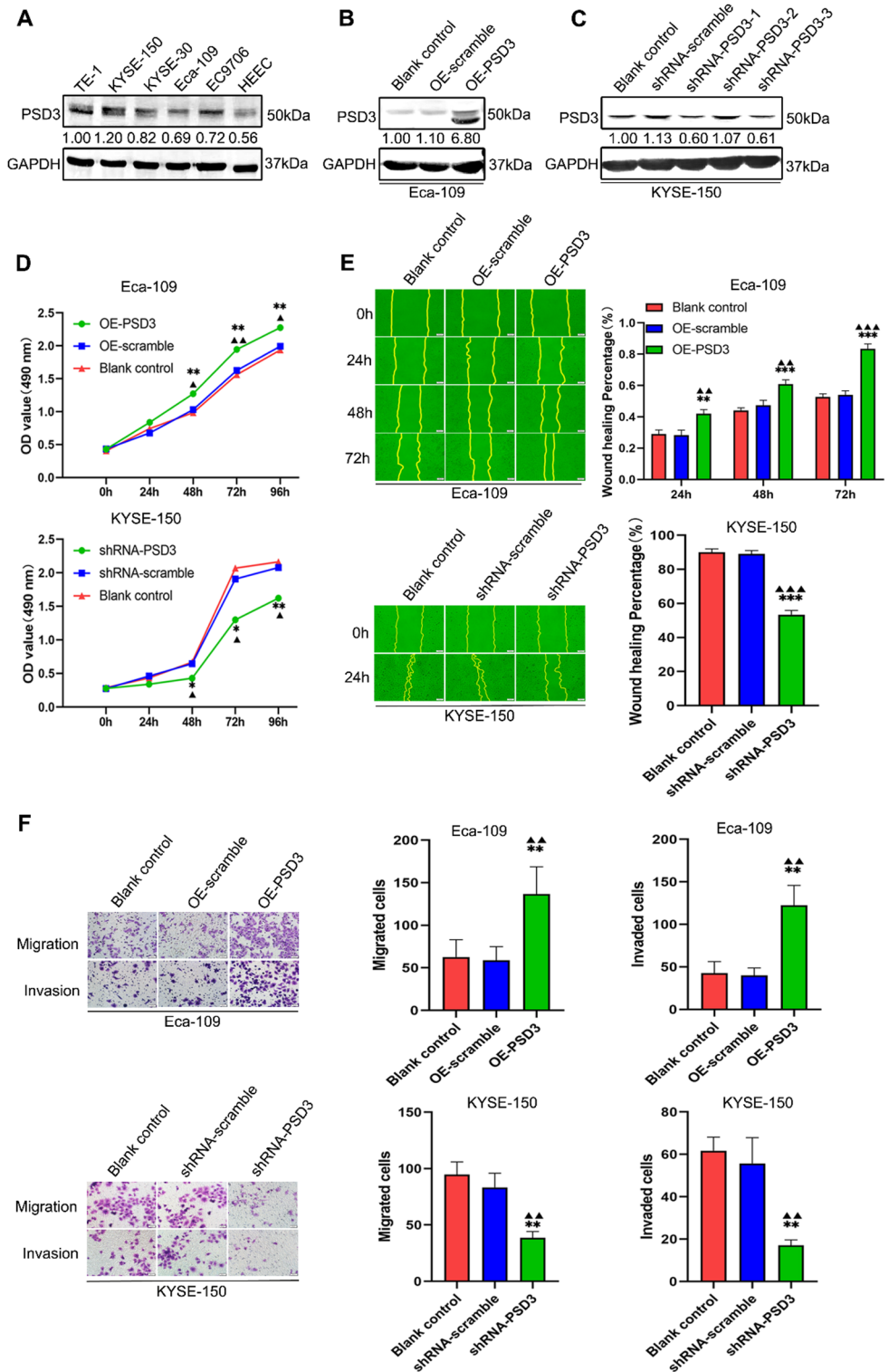


**Fig. 2.** PSD3 promotes proliferation, migration, and invasion of ESCC cells in vitro. **A**, Endogenous expression of PSD3 in ESCC cell lines. **B, C**, Assayed was the variation of PSD3 expression in Eca-109 cells transfected with Lv-overexpress-PSD3 and in KYSE-150 cells transfected with Lv-shRNA-PSD3 by Western blot. **D**, Assayed was the proliferation by MTT assay. **E**, Assayed was the migration by Wound Healing method; Magnification: 100×, scale bar represents 100 μm correspondingly. **F**, Assayed were the migration and invasion by Transwell assay; Magnification: 200×, scale bar represents 50 μm correspondingly. \* represents comparison with the Blank control, \* $p < 0.05$ , \*\* $p < 0.01$ , and \*\*\* $p < 0.001$ ; ▲ represents comparison with scramble, ▲  $p < 0.05$ , ▲▲  $p < 0.01$ , and ▲▲▲  $p < 0.001$ .

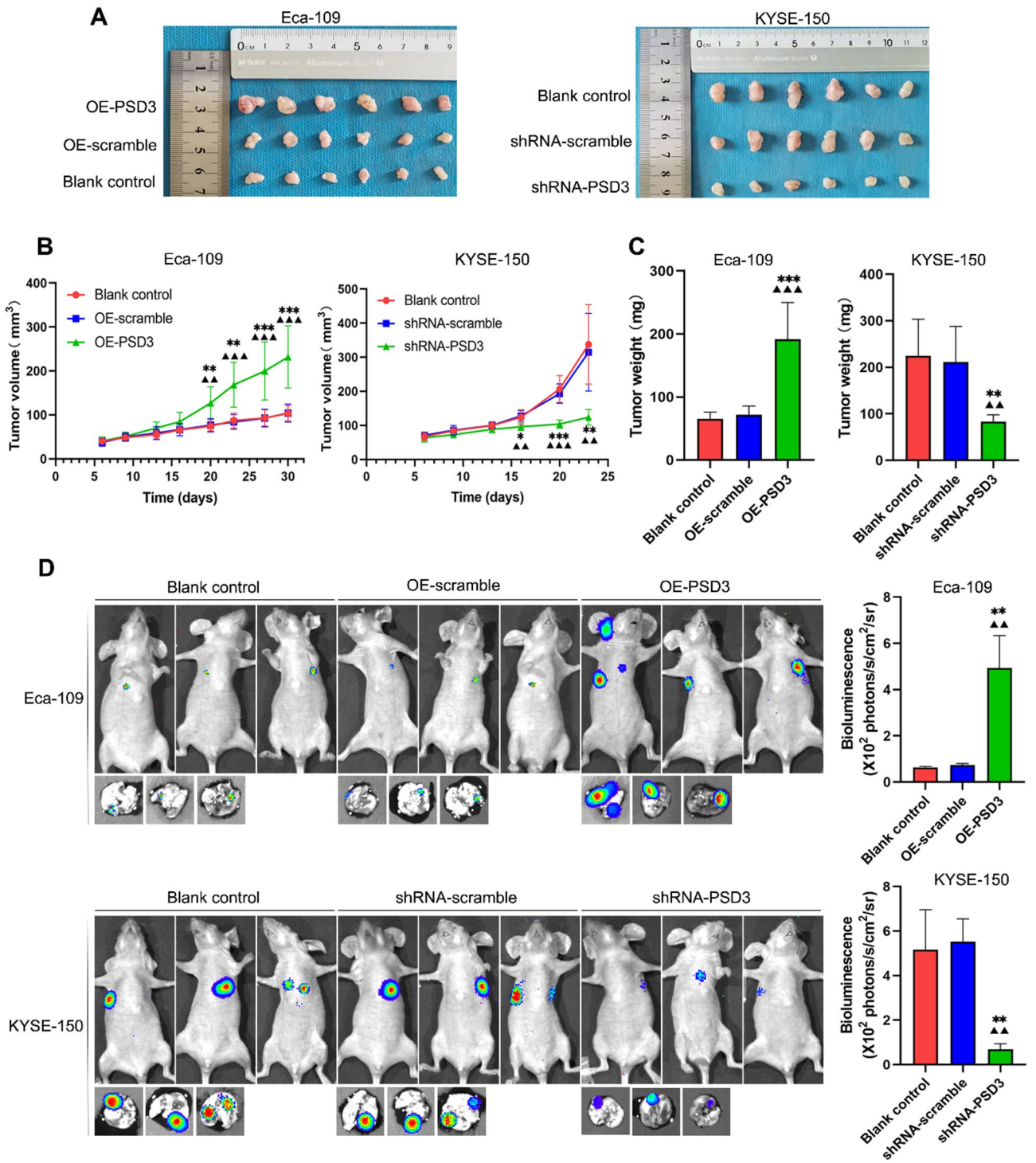


**Fig. 3.** PSD3 promotes the growth and metastasis of ESCC tumors in vivo. **A**, Images of tumor lesions ( $n = 6$ ). **B**, Tumor growth curves of mice ( $n = 6$ ). **C**, Shown were the histograms analyzing the weight of tumor lesions. **D**, Lung metastases in nude mice were detected by bioluminescence imaging and quantified ( $n = 3$ ). \*represents comparison with the Blank control,  $*p < 0.05$ ,  $**p < 0.01$ , and  $***p < 0.001$ ;  $\blacktriangle$  represents comparison with scramble,  $\blacktriangle p < 0.05$ ,  $\blacktriangle\blacktriangle p < 0.01$ , and  $\blacktriangle\blacktriangle\blacktriangle p < 0.001$ .

PSD3 expression was evaluated in the ESCC tissue microarray HESo180Su08 in this study. We first analyzed the association between PSD3 and PKM2 expression in the 80 ESCC clinical cases overlapping between the two chips, and the results showed that the expression of PSD3 and PKM2 was associated at the clinical tissue level in ESCC ( $P = 0.036$ ; Supplementary Table 1). Next, the results showed that PKM2, especially dimeric PKM2 (R399E and K367M), upregulated PSD3 (Fig. 5A, B). To investigate the potential interaction between PKM2 and

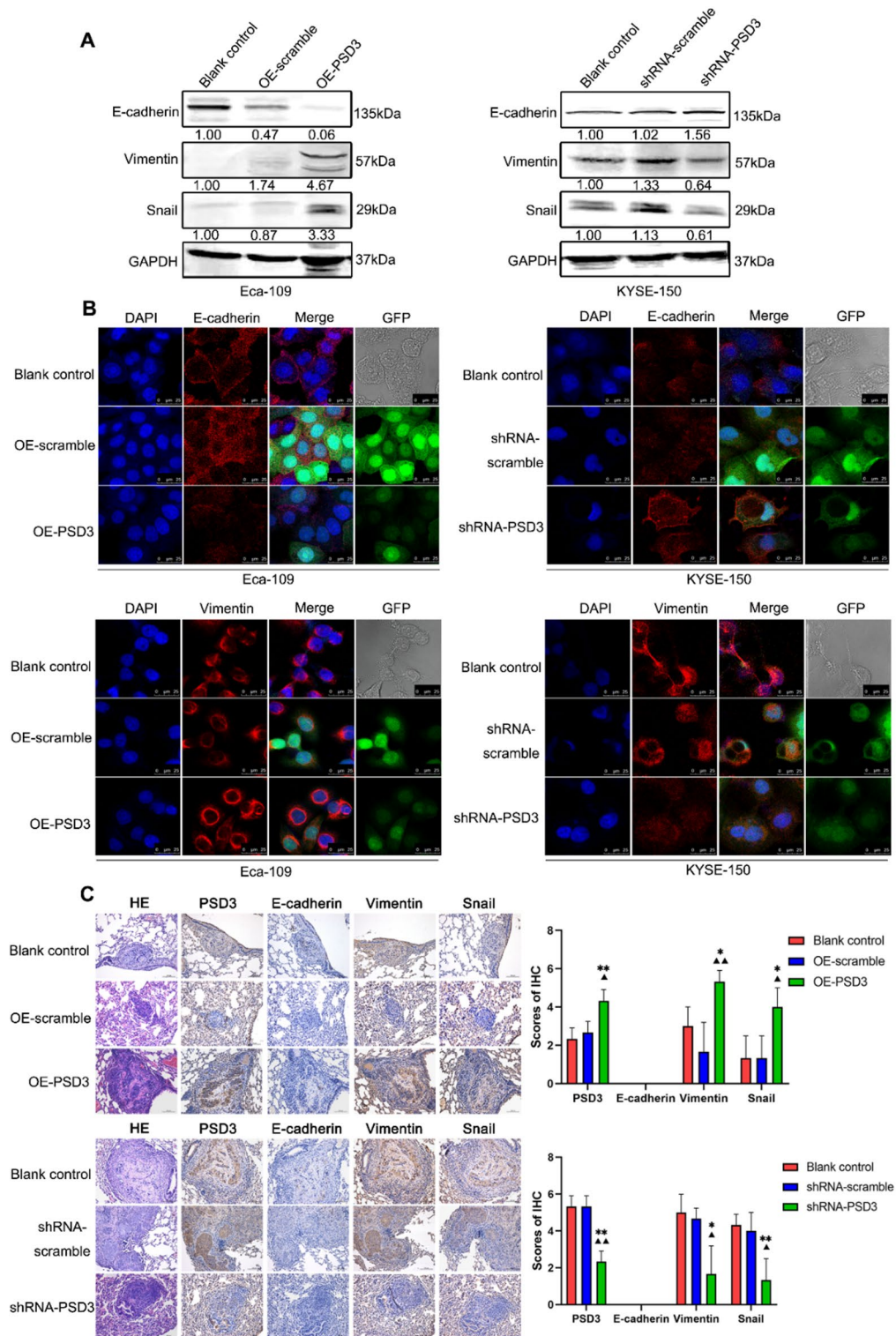


**Fig. 4.** PSD3 facilitates the EMT process of ESCC. **A, B,** Assessed was the variation of E-cadherin, Vimentin and Snail expression in Eca-109 cells or KYSE-150 cells after PSD3 was being artificially manipulated by Western blot and Immunofluorescence; Magnification: 400×, scale bar represents 25 μm correspondingly. **C,** Assessed was the variation of PSD3, E-cadherin, Vimentin and Snail expression in lung metastases by IHC; Magnification: 100×, scale bar represents 100 μm correspondingly. \* represents comparison with the Blank control,  $p < 0.05$  and  $**p < 0.01$ ; ▲ represents comparison with scramble, ▲  $p < 0.05$  and ▲▲  $p < 0.01$ .

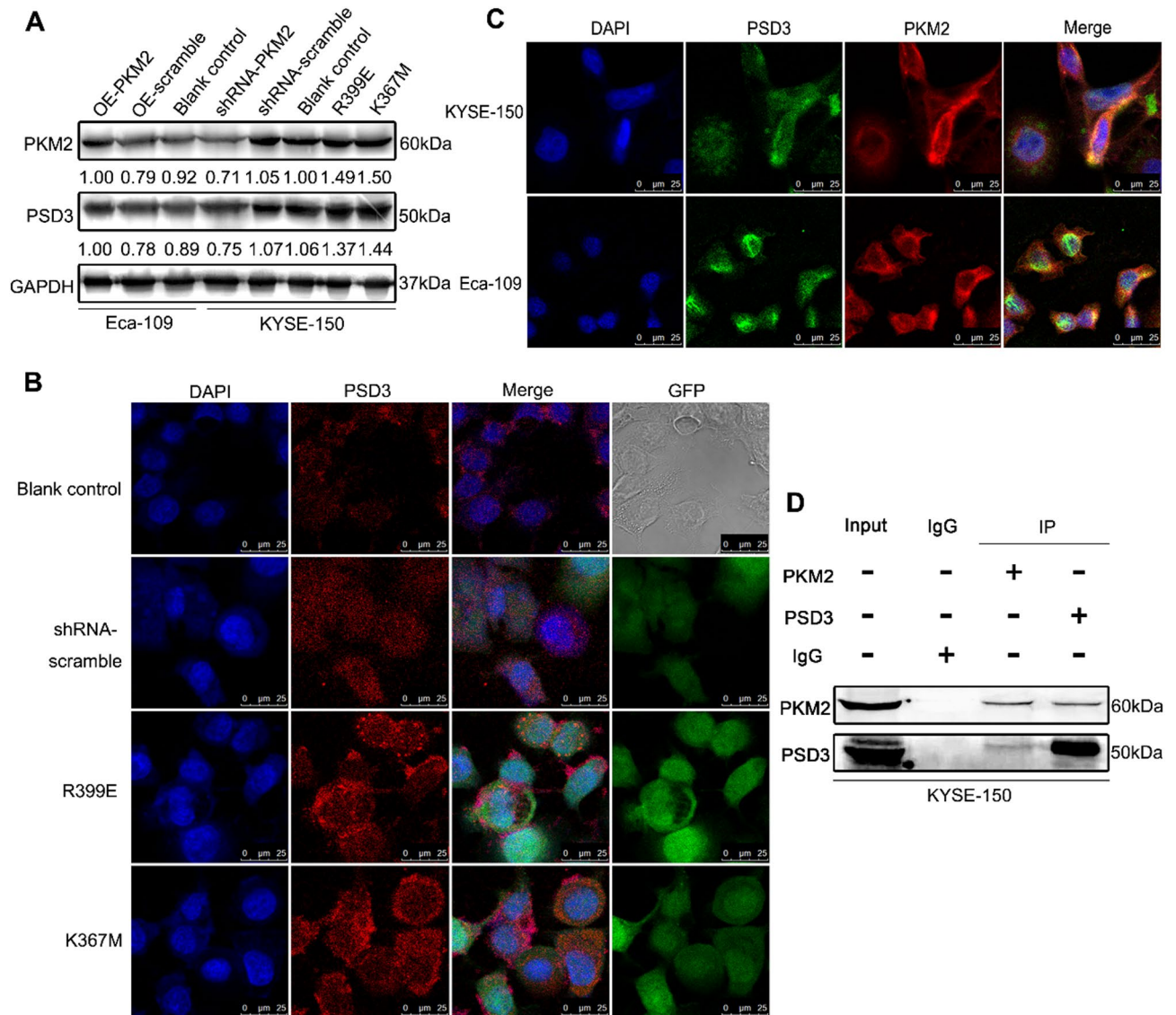


**Fig. 5.** PSD3 is directly regulated by PKM2. **A**, PSD3 expression was verified by Western blot after PKM2 overexpression, knockdown and mutation. **B**, PSD3 expression in PKM2 mutants was detected by Immunofluorescence; Magnification: 400 $\times$ , scale bar represents 25  $\mu$ m correspondingly. **C**, Immunofluorescence of nuclei (DAPI, blue), PSD3 (green) and PKM2 (red) in KYSE-150 and Eca-109 cells; Magnification: 400 $\times$ , scale bar represents 25  $\mu$ m correspondingly. **D**, Interaction between PKM2 and PSD3, as shown by Co-Immunoprecipitation (Co-IP) assay.

PSD3, we first performed immunofluorescence assays. Confocal microscopy revealed colocalization of PKM2 and PSD3 in the cytoplasm (Fig. 5C). In addition, the coimmunoprecipitation (Co-IP) assay showed that PKM2 and PSD3 bound directly to each other (Fig. 5D). Together, the data we obtained indicate that PSD3 is directly regulated by PKM2.

## Discussion

ESCC is one of the most fatal malignancies worldwide. Despite advances in clinical and preclinical research, the prognosis of ESCC is still poor, and the underlying mechanisms of ESCC progression remain unclear. In the present investigation, PSD3 was observed to be highly expressed in ESCC tissues and associated with lymph node metastasis. PSD3 significantly promoted ESCC growth and metastasis in vitro and in vivo. Mechanistically, PSD3 is regulated by PKM2 to promote ESCC progression via regulation of the EMT process. Our study is meaningful because it is the first study to investigate the clinicopathological and biological roles of PSD3 in ESCC.

To our knowledge, current studies of PSD3 in cancers are limited and have inconsistent results. PSD3 was originally identified by immunological screening of recombinant cDNA libraries obtained from hepatocellular carcinoma samples and has since been shown to be upregulated in colon cancer and downregulated in breast,

prostate, and ovarian cancers; glioblastoma; and endometrial carcinoma<sup>5,17</sup>. PSD3 is an oncogene that promotes proliferation, migration, invasion, and G1/S transition while inhibiting apoptosis in papillary thyroid cancer<sup>9</sup>. As seen from the above observations, the current understanding of and research on PSD3 are insufficient. The expression and role of PSD3 in ESCC are not clear. Here, we found that PSD3 levels were significantly higher in ESCC tissues than in adjacent nontumor epithelial tissues and that ESCC patients with high expression levels of PSD3 were more likely to develop lymph node metastasis than those with low expression levels of PSD3. This suggests that PSD3 acts as an oncogene in ESCC, and this role was further demonstrated by *in vitro* and *in vivo* experiments, which revealed that PSD3 promotes ESCC growth and metastasis. It should be noted that the prognostic evaluation of PSD3 in this study was limited to overall survival analysis due to the absence of systematically documented disease-free survival and recurrence data in our retrospective cohort, which may constrain our understanding of PSD3's prognostic value in ESCC. However, the mechanisms by which PSD3 participates in ESCC progression are poorly understood.

PKM2, a rate-limiting enzyme in the last step of glycolysis, has been shown to be highly expressed in malignant tumor tissues and associated with poor prognosis through meta-analyses<sup>14,15,18–21</sup>. These properties were also demonstrated in ESCC tissues in our previous study<sup>16</sup>. Therefore, PKM2 may be considered a specific diagnostic and therapeutic target in ESCC. Several studies have attracted our attention; these studies showed that the R399E mutant, with the preferential dimeric form of PKM2, and the K367M mutant of PKM2, without pyruvate kinase activity, significantly promote tumor growth<sup>22–25</sup>. Therefore, to further reveal the mechanism that promotes ESCC progression when PKM2 plays a role in protein kinase activity, differentially expressed proteins between ESCC cells expressing the R399E mutant or K367M mutant and wild-type PKM2 were screened in this study. Excitingly, PSD3 was found to be significantly upregulated in cells expressing PKM2 mutants, suggesting that PSD3 may be an important target that interacts with PKM2 and affects malignant phenotypes of ESCC cells. Therefore, the relationship between PSD3 and PKM2 needs to be further explored.

Thus far, four physical interaction partners (MX1<sup>26</sup>, MLH<sup>27</sup>, PMS2<sup>27</sup>, and ARAP1<sup>28</sup>), one highly probable interaction partner (Dyn2<sup>6</sup>), and one genetic interaction partner (TP53<sup>29</sup>) have been identified for PSD3. The interaction between PSD3 and PKM2 has not been reported. This study demonstrated for the first time that PKM2 and PSD3 bind to each other in the cytoplasm through Co-IP assays. While the Co-IP data support their physical interaction, it should be noted that this approach has inherent limitations in detecting weak or transient interactions due to antibody affinity issues and potential complex dissociation during washing steps. Nevertheless, the consistent colocalization of PKM2 and PSD3 in the cytoplasm by immunofluorescence microscopy strengthens this finding. Further structural studies (e.g., crystallography or crosslinking mass spectrometry) will be needed to precisely map the binding interfaces. There are binding sites between PKM2 and PSD3, and PKM2 directly regulates PSD3 to promote the proliferation, migration and invasion of ESCC cells.

In the past, our knowledge of PSD3 was limited to the observation that PSD3 was able to restore the binding of GTP to ARF6 to change ARF6 from a deactivated state to an active state by removing GDP from ARF6<sup>30,31</sup>. Through our study, we learned that PSD3 is involved in nonglycolytic functions of PKM2. Notably, while PKM2's metabolic roles in glycolysis have been extensively characterized, our findings reveal a novel kinase-dependent regulation of PSD3 that operates independently of its canonical metabolic functions. Although PKM2 has been reported to promote the malignant phenotype of ESCC cells, most studies have focused on the role of its pyruvate kinase activity, while the role of its protein kinase activity is not well understood<sup>32–35</sup>. This knowledge gap underscores the significance of our discovery that dimeric PKM2 (R399E/K367M mutants) phosphorylates PSD3 to initiate oncogenic signaling. Therefore, based on our results, we believe that in the cytoplasm of ESCC cells, dimeric PKM2 directly binds to PSD3, upregulates the expression of PSD3, promotes the targeting of PSD3 to the plasma membrane, further increases the level of GTP-bound ARF6, and thus promotes the progression of ESCC. We acknowledge that the metabolic effects of PSD3 regulation require comprehensive elucidation, but notably, proteomic analysis of PKM2 mutant-expressing cells suggests that the PKM2-PSD3 axis may represent a signaling pathway distinct from metabolic reprogramming. Future studies investigating potential crosstalk between PSD3-mediated ARF6 activation and metabolic pathways would provide valuable mechanistic insights.

Notably, our mechanistic studies reveal that dimeric PKM2 promotes ESCC progression through upregulation of PSD3, which subsequently enhances ARF6 activation and drives EMT. While bulk transcriptome analysis (GEPIA) showed there is a positive correlation between PSD3 and *CDH1* in squamous cell carcinomas, our functional assays in ESCC models demonstrated that PSD3 protein promotes E-cadherin degradation. This apparent discrepancy likely stems from three key factors: (I) Tumor microenvironmental heterogeneity in bulk samples obscures cell-autonomous effects observed in pure ESCC cultures; (II) PKM2-mediated PSD3 post-translationally reverses its transcriptional association with E-cadherin; and (III) Unstratified ESCA samples in GEPIA may mask ESCC-specific regulation. Importantly, the PKM2-PSD3-ARF6 axis represents a non-canonical pathway independent of PKM2's metabolic functions, as evidenced by sustained EMT promotion in glycolytic-inhibited ESCC cells. These findings not only resolve the apparent contradiction between omics and experimental data but also highlight the importance of studying post-translational regulation in tumor biology.

In conclusion, our study demonstrates that PSD3 can promote the proliferation, migration, invasion and metastasis of ESCC cells both *in vitro* and *in vivo*. Mechanistically, PKM2 can directly upregulate PSD3, thus promoting the EMT process in ESCC. These findings may prove clinically useful for developing a new therapeutic target for ESCC progression.

## Materials and methods

### Cell lines and cell culture

The human normal esophageal epithelial cell line HEEC and ESCC cell lines, such as Eca-109, EC9706, KYSE-150, KYSE-30 and TE-1, were obtained from Saiao Biomedical Technology Co., Ltd. (Xinjiang, China). All cells were maintained in Roswell Park Memorial Institute (RPMI) 1640 medium (Gibco) supplemented with 10%

fetal bovine serum (FBS; Gibco) and 1% penicillin-streptomycin at 37 °C. The cell lines have been tested and authenticated by STR (Short Tandem Repeat).

### Lentiviral transduction

Lentiviral vectors for PSD3 and PKM2 knockdown and overexpression and for PKM2 mutation were constructed by Shanghai Gene Pharma Co., Ltd. (Shanghai, China). For infection, tumor cells were incubated with lentiviruses in the presence of polybrene (5 µg/mL) and enhanced infection solution. After 72 h, all fluorescent cells were sorted via flow cytometry (FCM), and the transduction efficiency was evaluated via Western blotting.

### Proteomics

Samples in lysis buffer (Thermo) were sonicated three times on ice using a high-intensity ultrasonic processor (Scientz). The remaining debris was removed by centrifugation at 12,000 × g and 4 °C for 10 min. Finally, the supernatant was collected, and the protein concentration was determined. For digestion, proteins were reduced with 5 mM dithiothreitol (Sigma) for 30 min at 56 °C and alkylated with 11 mM iodoacetamide (Sigma) for 15 min at room temperature in the dark. Finally, trypsin (Promega) was added. Peptides were desalted on a Strata X C18 SPE column (Phenomenex) and vacuum-dried. Peptides were reconstituted in 0.5 M TEAB (Sigma) and processed according to the manufacturer's protocol for the TMT kit/iTRAQ kit (Thermo). The tryptic peptides were fractionated by high-pH reverse-phase HPLC using a Thermo Betasil C18 column (5 µm particles, 10 mm ID, 250 mm length). The tryptic peptides were dissolved in 0.1% formic acid (Fluka) and directly loaded onto an in-house-developed reversed-phase analytical column (15 cm length, 75 µm i.d.). The peptides were exposed to an NSI source, and tandem mass spectrometry (MS/MS) was then performed in a Q Exactive™ Plus instrument (Thermo) coupled online to the UPLC system. The resulting MS/MS data were processed using the MaxQuant search engine (v.1.5.2.8 <http://www.maxquant.org/>).

### Immunohistochemistry (IHC)

The protocol for the research project was approved by the Medical Ethics Committee of the First Affiliated Hospital of Xinjiang Medical University and conformed to the tenets of the Declaration of Helsinki. ESCC tissue microarrays were synthesized by Shanghai Outdo Biotechnology (catalog numbers: HEsoS180Su08, HEso-Squ180Sur-01). There were 80 overlapping cases between the two microarrays. The ESCC tissue microarray (HEsoS180Su08) was incubated at 60 °C for 16 h, and the slides were then dewaxed in an alcohol gradient. The tissue chips were then immersed first in 3% H<sub>2</sub>O<sub>2</sub> and then in 0.01 M citrate buffer and heated in a microwave at 95 °C for 10 min. Next, the tissue microarray was incubated with normal goat serum for 30 min, washed with phosphate buffer solution (PBS), and incubated with a rabbit polyclonal anti-PSD3 antibody (catalog number: ab62194, 1:150 dilution; Abcam) in a humidified box at 4 °C overnight. The tissue microarray was incubated with the secondary antibody at 37 °C for 60 min (catalog number: ZLI-9032, Zhongshan Jinqiao Biotechnology), and staining was visualized by careful application of a 3'-diaminobenzidine substrate kit (catalog number: ZLI-9018, Zhongshan Jinqiao Biotechnology) for 1 min under a microscope. The evaluation included determination of the staining intensity and the percentage of positive cells. Four scores were assigned for the staining intensity (0, no staining; 1, weak staining; 2, moderate staining; and 3, strong staining) and for the percentage of positive cells (0, < 10%; 1, 10–25%; 2, 25–50%; and 3, > 50%). The scores for the staining intensity and the percentage of positive cells were summed to calculate the immunoreactive score (IRS). Finally, the specimens were divided into two groups according to protein levels: low expression, IRS 0–2; high expression, IRS 3–6.

### Western blot analysis

Samples were grouped and lysed with radioimmunoprecipitation assay (RIPA) buffer (catalog number: 899001; Thermo) containing a phosphatase inhibitor (catalog number: 78442; Thermo). The concentration of total protein was determined by a BCA kit (Solarbio, Beijing, China). Proteins were separated on a 10% SDS-PAGE gel and were then transblotted to PVDF membranes. Then, the membranes were blocked with 5% skim milk for 2 h and incubated with the primary antibodies listed below overnight at 4 °C and with secondary antibodies for 2 h. Novex® AP Chromogenic substrate (BCIP/NBT) was used to visualize protein bands. ImageJ software (1.8.0, USA) was used to semiquantitatively analyze the protein bands. The primary antibodies used were as follows: anti-PKM2 (catalog number: 4053 S, 1:1,000; Cell Signaling Technology), anti-p-PKM2 (catalog number: 3827 S, 1:1,000; Cell Signaling Technology), anti-PSD3 (catalog number: ab62194, 1:500; Abcam), anti-E-cadherin (catalog number: 3195 S, 1:1,000; Cell Signaling Technology), anti-Vimentin (catalog number: 5741 S, 1:1,000; Cell Signaling Technology), anti-Snail (catalog number: 3879 S, 1:1,000; Cell Signaling Technology) and anti-glyceraldehyde 3-phosphate dehydrogenase (GAPDH) (catalog number: ab8245, 1:10,000; Abcam).

### MTT assay

ESCC cells were seeded in 96-well plates at a density of 5 × 10<sup>3</sup> cells/well. At the designated time points, the cells were incubated with 90 µL of fresh medium and 10 µL of 3-(4,5-dimethyl-2-thiazolyl)-2,5-diphenyl-2-H-tetrazolium bromide (MTT; Solarbio, Beijing, China) for 4 h at 37 °C. The reaction was terminated by removal of the culture medium followed by the addition of 110 µL of DMSO for 20 min to dissolve the formazan product. Finally, absorbance values were measured at 490 nm.

### Wound healing assay

ESCC cells were seeded in 6-well plates at a density of 3 × 10<sup>5</sup> cells per well and cultured in complete medium containing 10% FBS until reaching 80–90% confluency. To minimize proliferation effects, the cells were then serum-starved by replacing the medium with 1% FBS medium for 24 h prior to wounding. A straight scratch with consistent angle and width was created in each well using a sterile pipette tip. Following wound induction,

the cells were maintained in 1% FBS medium. Images were acquired at three predefined fields per well using fixed coordinates at each time point (0/24/48/72 h). Wound areas were quantified using ImageJ software, and the migration rate was calculated as:  $[(A_0 - A_t)/A_0] \times 100\%$ , where  $A_0$  represents the initial wound area (0 h) and  $A_t$  denotes the area at time  $t$ . Experiments were independently repeated three times (scale bar: 100  $\mu\text{m}$ ).

### Transwell migration and invasion assays

For the invasion assay, 8  $\mu\text{m}$  pore size membranes in a Transwell system (Corning, New York) were precoated with 50  $\mu\text{L}$  of Matrigel (1:8 dilution; BD, Bedford, MA). For the migration assay, Matrigel was not required. Cells ( $5 \times 10^4$  per well) were seeded into the upper chambers in 200  $\mu\text{L}$  of medium without FBS. The lower chambers contained RPMI 1640 supplemented with 10% FBS. Then, the plates were placed in a 37  $^\circ\text{C}$  cell incubator for 24 h. The cells were fixed with 4% paraformaldehyde and stained with 0.1% crystal violet for 15 min. Cells that did not penetrate through the membrane were gently removed by wiping with cotton swabs, and the plates were then washed with PBS. Invaded cells and migrated cells were counted in five random areas and images were acquired under a microscope (50  $\mu\text{m}$ ).

### Animal experiments

The animal experiments were approved by the Medical Ethics Committee of the First Affiliated Hospital of Xinjiang Medical University. Female BALB/c nude mice (Charles River, Beijing, China) aged 4–6 weeks were used to establish a subcutaneous tumor model and a tail vein injection model. Eca-109 cells ( $6 \times 10^6$  for subcutaneous inoculation and  $2 \times 10^6$  for intravenous inoculation) transfected with Lv-overexpress-PSD3 or Lv-overexpress-scramble and KYSE-150 cells ( $3 \times 10^6$  for subcutaneous inoculation and  $5 \times 10^5$  for intravenous inoculation) transfected with Lv-shRNA-PSD3 or Lv-shRNA-scramble were injected subcutaneously or intravenously into nude mice. In the subcutaneous injection model, tumor formation was observed on the 6th day after cell injection, and tumor growth was monitored twice a week. The tumor volume was calculated from measurements of 2 diameters of the individual tumor base using the following formula: tumor volume ( $\text{mm}^3$ ) = (length  $\times$  width<sup>2</sup>)  $\times$  0.5. In the tail vein injection model, pulmonary metastasis was observed every 7 days after cell injection. Thirty-eight days after cell injection, bioluminescence imaging was performed to observe the metastasis of cancer cells (IVIS<sup>®</sup> Lumina LT, PerkinElmer), and signals were analyzed using Living Image<sup>®</sup> Software 4.4 for the IVIS<sup>®</sup> Spectrum (PerkinElmer). Finally, the nude mice were euthanized with an intraperitoneal injection of an overdose of pentobarbital dissolved in saline solution (100 mg per kilogram of animal body weight), according to the American Veterinary Medical Association guidelines for the euthanasia of animals. Resected tumor lesions were formalin-fixed, paraffin-embedded, and stained with hematoxylin and eosin to confirm derivation from ESCC cells. All animals received care in accordance with the recommendations of the National Institutes of Health Guide for Care and Use of Laboratory Animals and adhered to the ARRIVE guidelines.

### Immunofluorescence

Cells were fixed with 4% paraformaldehyde at 4  $^\circ\text{C}$  for 30 min and then subjected to treatment with 0.5% Triton X-100 at room temperature for 20 min. The cells were blocked in PBS with 2% BSA (Sigma) at 37  $^\circ\text{C}$  for 30 min and incubated with primary antibodies overnight at 4  $^\circ\text{C}$ . The cells were then incubated with Alexa Fluor-conjugated secondary antibodies (Alexa Fluor 488 and Alexa Fluor 594; Thermo) for 2 h at room temperature in the dark. 2-(4-Amidinophenyl)-6-indolecarbamide dihydrochloride (DAPI; catalog number: 28718-90-3, 10  $\mu\text{g}/\text{mL}$ ; Sigma) was then used to counterstain nuclei for 30 min at room temperature, and images were acquired with a laser scanning confocal microscope (LSM710, Carl Zeiss AG) at a magnification of 400 $\times$ . The primary antibodies used were as follows: anti-PKM2 (catalog number: 60268-1-Ig, 1:100; Proteintech), anti-PSD3 (catalog number: ab62194, 1:100; Abcam), anti-E-cadherin (catalog number: 3195 S, 1:100; Cell Signaling Technology), and anti-Vimentin (catalog number: 5741 S, 1:100; Cell Signaling Technology).

### Coimmunoprecipitation (Co-IP)

Co-IP was carried out according to the instructions included in the assay kit (catalog number: Pierce 26149, Thermo). First, total protein was extracted from cell lysates, and 500  $\mu\text{g}$  of total protein was mixed with 2  $\mu\text{g}$  of a primary antibody or IgG and incubated overnight at 4  $^\circ\text{C}$  with rotation. The protein beads in the kit were added to the mixture and incubated at room temperature for 2 h with rotation. Subsequently, the beads were washed using IP buffer three times. Sample buffer (2 $\times$ ) was mixed with the beads, and the mixture was boiled for 5 min. The supernatant was prepared for Western blot analysis. The primary antibodies used were as follows: anti-PKM2 (catalog number: 4053 S; Cell Signaling Technology) and anti-PSD3 (catalog number: ab62194; Abcam).

### GEPIA (Gene expression profiling interactive Analysis)

The GEPIA (<http://GEPIA.cancer-pku.cn/index.html>) online database contains research data both from TCGA and GTEx, including RNA sequencing data of 9736 tumor samples and 857 normal samples.

### Statistical analysis

All experiments were performed independently at least three times unless otherwise stated. Data are expressed as the mean  $\pm$  standard deviation (SD) values. A two-tailed independent samples  $t$  test was used to analyze the significance of differences between two groups of normally distributed data; for comparisons among more than two groups, univariate analysis of variance followed by post hoc analysis with the LSD test was adopted to assess the significance of differences among the groups. For categorical data, the  $\chi^2$  test was utilized to analyze correlations between protein expression and clinicopathological parameters. In particular, when there were fewer than five categorical variables in the contingency table, Fisher's exact test was used. Survival analysis

was performed using the Kaplan–Meier method for analysis of overall prognosis. The correlation coefficient calculated with the chi-square test was used for correlation analysis of PKM2 and PSD3 expression. SPSS Statistics 17.0 software was used to analyze and process the experimental data, and GraphPad Prism 8.0 software was employed to generate the various kinds of plots shown.  $p < 0.05$  was regarded as significant in all tests.

## Data availability

The datasets used and/or analysed during the current study available from the corresponding author on reasonable request.

Received: 28 July 2024; Accepted: 3 June 2025

Published online: 02 July 2025

## References

- Wu, X., Zhang, H., Sui, Z., Wang, Y. & Yu, Z. The biological role of the CXCL12/CXCR4 axis in esophageal squamous cell carcinoma. *Cancer Biology Med.* <https://doi.org/10.20892/j.issn.2095-3941.2020.0140> (2021).
- Wu, H. et al. Clinical benefit of First-Line programmed death-1 antibody plus chemotherapy in low programmed cell death ligand 1-Expressing esophageal squamous cell carcinoma: A post hoc analysis of JUPITER-06 and Meta-Analysis. *J. Clin. Oncology: Official J. Am. Soc. Clin. Oncol.* **JCO2201490** <https://doi.org/10.1200/jco.22.01490> (2022).
- Hirano, H. & Kato, K. Systemic treatment of advanced esophageal squamous cell carcinoma: chemotherapy, molecular-targeting therapy and immunotherapy. *Jpn J. Clin. Oncol.* **49**, 412–420. <https://doi.org/10.1093/jco/hyz034> (2019).
- Sakagami, H. The EFA6 family: guanine nucleotide exchange factors for ADP ribosylation factor 6 at neuronal synapses. *Tohoku J. Exp. Med.* **214**, 191–198. <https://doi.org/10.1620/tjem.214.191> (2008).
- Kanamarlapudi, V. Exchange factor EFA6R requires C-terminal targeting to the plasma membrane to promote cytoskeletal rearrangement through the activation of ADP-ribosylation factor 6 (ARF6). *J. Biol. Chem.* **289**, 33378–33390. <https://doi.org/10.1074/jbc.M113.534156> (2014).
- Okada, R. et al. Activation of the small G protein Arf6 by Dynamin2 through guanine nucleotide exchange factors in endocytosis. *Sci. Rep.* **5**, 14919. <https://doi.org/10.1038/srep14919> (2015).
- Wang, Y. et al. Large scale identification of human hepatocellular carcinoma-associated antigens by autoantibodies. *J. Immunol. (Baltimore Md. : 1950)*. **169**, 1102–1109. <https://doi.org/10.4049/jimmunol.169.2.1102> (2002).
- Hongu, T. et al. Arf6 regulates tumour angiogenesis and growth through HGF-induced endothelial  $\beta 1$  integrin recycling. *Nat. Commun.* **6**, 7925. <https://doi.org/10.1038/ncomms8925> (2015).
- Jin, L. et al. PSD3 is an oncogene that promotes proliferation, migration, invasion, and G1/S transition while inhibits apoptotic in papillary thyroid cancer. *J. Cancer.* **12**, 5413–5422. <https://doi.org/10.7150/jca.60885> (2021).
- Thomassen, M., Tan, Q. & Kruse, T. Gene expression meta-analysis identifies chromosomal regions and candidate genes involved in breast cancer metastasis. *Breast Cancer Res. Treat.* **113**, 239–249. <https://doi.org/10.1007/s10549-008-9927-2> (2009).
- Pils, D. et al. Five genes from chromosomal band 8p22 are significantly down-regulated in ovarian carcinoma: N33 and EFA6R have a potential impact on overall survival. *Cancer* **104**, 2417–2429. <https://doi.org/10.1002/cncr.21538> (2005).
- Zahra, K., Dey, T., Ashish, Mishra, S. & Pandey, U. Pyruvate kinase M2 and cancer: the role of PKM2 in promoting tumorigenesis. *Front. Oncol.* **10**, 159. <https://doi.org/10.3389/fonc.2020.00159> (2020).
- Puckett, D., Alquraishi, M., Chowanadisai, W. & Bettaieb, A. The role of PKM2 in metabolic reprogramming: insights into the regulatory roles of Non-Coding RNAs. *Int. J. Mol. Sci.* **22** <https://doi.org/10.3390/ijms22031171> (2021).
- Wang, C., Wang, J., Chen, Z., Gao, Y. & He, J. Immunohistochemical prognostic markers of esophageal squamous cell carcinoma: a systematic review. *Chin. J. cancer.* **36** <https://doi.org/10.1186/s40880-017-0232-5> (2017).
- Zhu, H. et al. Pyruvate kinase M2 (PKM2) expression correlates with prognosis in solid cancers: a meta-analysis. *Oncotarget* **8**, 1628–1640. <https://doi.org/10.18632/oncotarget.13703> (2017).
- Ma, R. et al. PKM2-regulated STAT3 promotes esophageal squamous cell carcinoma progression via TGF- $\beta 1$ -induced EMT. *J. Cell. Biochem.* <https://doi.org/10.1002/jcb.28434> (2019).
- Wang, A., Guo, H. & Long, Z. Integrative analysis of differently expressed genes reveals a 17-Genes prognosis signature for endometrial carcinoma. *Biomed. Res. Int.* **2021** (4804694). <https://doi.org/10.1155/2021/4804694> (2021).
- Wu, J. et al. Pyruvate kinase M2 overexpression and poor prognosis in solid tumors of digestive system: evidence from 16 cohort studies. *Onco Targets Ther.* **9**, 4277–4288. <https://doi.org/10.2147/ott.S106508> (2016).
- Yang, Y. et al. Prognostic significance of metabolic enzyme pyruvate kinase M2 in breast cancer: A meta-analysis. *Medicine* **96**, e8690. <https://doi.org/10.1097/md.00000000000008690> (2017).
- Li, H., Yan, M., Wu, X., Wang, Y. & Huang, L. Expression and clinical significance of pyruvate kinase M2 in breast cancer: A protocol for meta-analysis and bioinformatics validation analysis. *Medicine* **100**, e25545. <https://doi.org/10.1097/md.00000000000025545> (2021).
- Wang, Y. et al. Prognostic value of Glycolysis markers in head and neck squamous cell carcinoma: a meta-analysis. *Aging* **13**, 7284–7299. <https://doi.org/10.18632/aging.202583> (2021).
- Hsu, M. et al. Extracellular PKM2 induces cancer proliferation by activating the EGFR signaling pathway. *Am. J. Cancer Res.* **6**, 628–638 (2016).
- Chen, T. et al. Mutations in the PKM2 exon-10 region are associated with reduced allostery and increased nuclear translocation. *Commun. Biology.* **2**, 105. <https://doi.org/10.1038/s42003-019-0343-4> (2019).
- Gao, X., Wang, H., Yang, J., Liu, X. & Liu, Z. Pyruvate kinase M2 regulates gene transcription by acting as a protein kinase. *Mol. Cell.* **45**, 598–609. <https://doi.org/10.1016/j.molcel.2012.01.001> (2012).
- Mazurek, S. Pyruvate kinase type M2: a key regulator of the metabolic budget system in tumor cells. *Int. J. Biochem. Cell Biol.* **43**, 969–980. <https://doi.org/10.1016/j.biocel.2010.02.005> (2011).
- Brantis-de-Carvalho, C. et al. MxA interacts with and is modified by the sumoylation machinery. *Exp. Cell. Res.* **330**, 151–163. <https://doi.org/10.1016/j.yexcr.2014.10.020> (2015).
- Cannavo, E., Gerrits, B., Marra, G., Schlapbach, R. & Jiricny, J. Characterization of the interactome of the human MutL homologues MLH1, PMS1, and PMS2. *J. Biol. Chem.* **282**, 2976–2986. <https://doi.org/10.1074/jbc.M609989200> (2007).
- Yoon, H., Kales, S., Luo, R., Lipkowitz, S. & Randazzo, P. ARAP1 association with CIN85 affects epidermal growth factor receptor endocytic trafficking. *Biol. Cell.* **103**, 171–184. <https://doi.org/10.1042/bc20100154> (2011).
- Xie, L. et al. A synthetic interaction screen identifies factors selectively required for proliferation and TERT transcription in p53-deficient human cancer cells. *PLoS Genet.* **8**, e1003151. <https://doi.org/10.1371/journal.pgen.1003151> (2012).
- Chen, K., Hsu, J. & Lee, F. AMPK promotes Arf6 activation in a kinase-independent manner upon glucose starvation. *J. Cell. Sci.* **135** <https://doi.org/10.1242/jcs.259609> (2022).
- Ghosh, M. et al. CD13 tethers the IQGAP1-ARF6-EFA6 complex to the plasma membrane to promote ARF6 activation,  $\beta 1$  integrin recycling, and cell migration. *Sci. Signal.* **12** <https://doi.org/10.1126/scisignal.aav5938> (2019).

32. Xiaoyu, H. et al. The mTOR pathway regulates PKM2 to affect Glycolysis in esophageal squamous cell carcinoma. *Technol. Cancer Res. Treat.* **17**, 1533033818780063. <https://doi.org/10.1177/1533033818780063> (2018).
33. Wang, W. et al. METTL3 promotes tumour development by decreasing APC expression mediated by APC mRNA N-methyladenosine-dependent YTHDF binding. *Nat. Commun.* **12**, 3803. <https://doi.org/10.1038/s41467-021-23501-5> (2021).
34. Li, S. et al. Dihydroartemisinin represses esophageal cancer Glycolysis by down-regulating pyruvate kinase M2. *Eur. J. Pharmacol.* **854**, 232–239. <https://doi.org/10.1016/j.ejphar.2019.04.018> (2019).
35. Fu, J. et al. Hyperactivity of the transcription factor Nrf2 causes metabolic reprogramming in mouse esophagus. *J. Biol. Chem.* **294**, 327–340. <https://doi.org/10.1074/jbc.RA118.005963> (2019).

## Acknowledgements

This study was funded by the Natural Science Foundation of China (82260568), the Leading Talent Project of Scientific and Technological Innovation in Tianshan Talents Training Plan of Xinjiang Uygur Autonomous Region (2022TSYCLJ0031), the Major Research Project Incubation Program of Xinjiang Medical University (XY-D2024ZX02), the Natural Science Foundation of Xinjiang Uygur Autonomous Region (2023D01C97), the State Key Laboratory of Pathogenesis, Prevention and Treatment of High Incidence Diseases in Central Asia Fund, Urumqi, Xinjiang Uygur Autonomous Region (SKL-HIDCA-2024-43, SKL-HIDCA2024-SG4), the Xinjiang Uygur Autonomous Region “Tianchi Talents” Introduction Program-Young Doctoral Program for Qiqi Zhang, and Innovative team training project of the First Affiliated Hospital of Xinjiang Medical University (LXM).

## Author contributions

All authors contributed to the study conception and design. Material preparation, data collection and analysis were performed by Qiqi Zhang, Qing Liu, Shutao Zheng, Tao Liu, Yiyi Tan and Lifei Yang. The first draft of the manuscript was written by Qiqi Zhang, Xiaomei Lu and all authors commented on previous versions of the manuscript. All authors read and approved the final manuscript.

## Declarations

### Competing interests

The authors declare no competing interests.

### Ethics approval

This study was performed in line with the principles of the Declaration of Helsinki. Approval was granted by the Ethics Committee of First Affiliated Hospital of Xinjiang Medical University (permission no. 20160218-123).

### Additional information

**Supplementary Information** The online version contains supplementary material available at <https://doi.org/10.1038/s41598-025-05649-y>.

**Correspondence** and requests for materials should be addressed to X.L.

**Reprints and permissions information** is available at [www.nature.com/reprints](http://www.nature.com/reprints).

**Publisher’s note** Springer Nature remains neutral with regard to jurisdictional claims in published maps and institutional affiliations.

**Open Access** This article is licensed under a Creative Commons Attribution-NonCommercial-NoDerivatives 4.0 International License, which permits any non-commercial use, sharing, distribution and reproduction in any medium or format, as long as you give appropriate credit to the original author(s) and the source, provide a link to the Creative Commons licence, and indicate if you modified the licensed material. You do not have permission under this licence to share adapted material derived from this article or parts of it. The images or other third party material in this article are included in the article’s Creative Commons licence, unless indicated otherwise in a credit line to the material. If material is not included in the article’s Creative Commons licence and your intended use is not permitted by statutory regulation or exceeds the permitted use, you will need to obtain permission directly from the copyright holder. To view a copy of this licence, visit <http://creativecommons.org/licenses/by-nc-nd/4.0/>.

© The Author(s) 2025